

Fully Utilizing Contrast Enhancement on Lung Tissue as a Novel Basis Material for Lung Nodule Characterization by Multi-energy CT

Shaojie Chang^a, Yongfeng Gao^a, Marc J. Pomeroy^a, Ti Bai^b, Hao Zhang^c, Zhengrong Liang^{*d}
^a Department of Radiology, Stony Brook University, Stony Brook, NY 11794, USA; ^b Department of Radiation Oncology, University of Texas Southwestern Medical Centre, Dallas, TX 75390, USA; ^c Department of Medical Physics, Memorial Sloan Kettering Cancer Center, NY 10065, USA; ^d Departments of Radiology and Biomedical Engineering, Stony Brook University, Stony Brook, NY 11794, USA

ABSTRACT

Based on well-established X-ray physics in computed tomography (CT) imaging, the spectral responses of different materials contained in lesions are different, which brings richer contrast information at various energy bins. Hence, obtaining the material decomposition of different tissue types and exploring its spectral information for lesion diagnosis becomes extremely valuable. The lungs are housed within the torso and consist of three natural materials, i.e., soft tissue, bone, and lung tissue. To benefit the lung nodule differentiation, this study innovatively proposed to use lung tissue as one basis material along with soft tissue and bone. This set of basis materials will yield a more accurate composition analysis of lung nodules and benefit the following differentiation. Moreover, a corresponding machine learning (ML)-based computer-aided diagnosis framework for lung nodule classification is also proposed and used for evaluation. Experimental results show the advantages of the virtual monoenergetic images (VMIs) generated with lung tissue material over the VMIs without lung tissue and conventional CT images in differentiating the malignancy from benign lung nodules. The gain of 9.63% in area under the receiver operating characteristic curve (AUC) scores indicated that the energy-enhanced tissue features from lung tissue have a great potential to improve lung nodule diagnosis performance.

Keywords: Multi-energy CT reconstruction, Computer-aided diagnosis, Machine learning, Malignant and benign differentiation

1. INTRODUCTION

IN the conventional single energy CT, different tissue types can be represented by the linear attenuation coefficients (LACs). LACs are not unique for any given material and depend on the photon energies interacting with the material and the mass density of the material. Therefore, two different tissues may share similar intensity values, making it challenging to perform material decomposition based on the segmentation with the intensity values alone. Compared to the conventional single energy CT, additional measurements with a second or more energy (called multi-energy) allow the identification of two or three materials. Multi-energy CT also enables multiple materials (composition) analysis within the same region of interest, e.g., lesion. Based on well-established X-ray physics in CT imaging, the spectral responses of different materials contained in lesions are different, which brings richer contrast information at different energy bins. Hence, obtaining the material decomposition of different tissue types and exploring its spectral information for lesion diagnosis becomes extremely valuable.

The lungs as the primary organs of the respiratory system are essential for humans to breathe. Lung cancer is the leading cause of cancer death in the US. According to the report from World Health Organization, there are around 2.20 million deaths in 2020. CT has been recommended as an advanced non-invasive tool for cancer screening in the early stage, which provides fully three-dimensional (3D) information for volumetric-based lesion detection. Torso CT images consist of three natural materials, which are lung, bone, and soft tissue. To benefit the lung nodule differentiation, this study innovatively proposed to use lung tissue as one basis material along with soft tissue and

* Author to whom correspondence should be addressed: E-mail: Jerome.Liang@SUNYSB.EDU.

bone. This set of three basis materials will yield a more accurate composition analysis of lung nodule and benefit the following differentiation.

In dual-energy CT (DECT), the scanned object can be decomposed into two basis materials (e.g., bone and soft tissue) with two datasets, one at high and the other at low energy [1]. To analyze more than two materials, one straightforward strategy is to obtain an additional measurement at one more energy, which we called triple energy CT (TECT). And it could provide three decomposed materials reconstructed from the three datasets. In the previous application, when using triple spectrums to decompose three materials, two materials are natural and the third is usually injected contrast agent (e.g., bone, soft tissue, and iodine) [2]. In this study, we use triple spectrums to decompose all-natural tissues: lung tissue, soft tissue, and bone. In addition, we also explore using two spectrums to decompose three materials, which can further lower the radiation dose. This paper will describe the material decomposition with the novel set of basis materials in detail. Moreover, a machine learning (ML)-based computer-aided diagnosis (CADx) framework for lung nodule classification is also proposed, which is based on the data-driven deep learning-based convolutional neural network (DL-CNN) method.

The remainder of this paper is organized as follows. Section II will describe the material decomposition method and the proposed computer-aided diagnosis framework. Section III presents the experiment design and results. Discussion and conclusions are drawn in Sections IV and V.

2. METHODS

2.1 Material Decomposition

Considering the material composition, a linear attenuation coefficient (LAC) can be represented by R types of basis materials, e.g. soft tissue, bone, and so on. The LAC function $\mu_j(\varepsilon)$ at the j^{th} pixel of the image is decomposed as[3]:

$$\mu_j(\varepsilon) = \sum_{r=1}^R m_r(\varepsilon) \rho_{rj}, \quad (1)$$

where ρ_{rj} denotes the density of material r at the j^{th} pixel, $m_r(\varepsilon)$ represents the mass attenuation coefficient of material r at energy ε .

By the use of DECT, two basis materials of bone and soft tissue are usually considered as the basis materials in the material composition. From the decomposed basis materials of bone and soft tissue, a series of virtual monoenergetic images (VMIs) can be generated. As lungs become a major clinical concern, where the lung tissue has a distinct feature from the soft tissue, it is desirable to consider the lung tissue as a basis material in addition to the bone and soft tissue. This is the major motivation of this study. The material decomposition can be performed directly in the sinogram data domain or the image domain after the images are reconstructed from the sinogram data, where the image reconstruction is usually performed by a linear operator, such as FBP.

1) Image-domain material decomposition

Regarding the material decomposition in the image domain, Eq. (1) can be rewritten as,

$$\mu_j(\varepsilon) = \sum_{r=1}^R m_r(\varepsilon) \rho_{rj} = \sum_{r=1}^R m_r(\varepsilon) \rho_r f_{rj} = \sum_{r=1}^R \mu_r(\varepsilon) f_{rj}, \quad (2)$$

where ρ_r is the density of the material r and $\mu_r(\varepsilon)$ denotes linear attenuation coefficient of material r at energy ε . Notation f_{rj} is a unitless tissue fraction that quantifies the contribution of material r to attenuation in pixel j , which needs to be solved by the image domain decomposition methods. Theoretically, more unknowns need more equations to find the solution. For a conventional single energy spectral CT image, we only have one FBP CT image. For DECT, we have two FBP images from each of the two energy spectral data, respectively. From the two FBP images, we can obtain two basis material images. For TECT, e.g. 60kVp, 100kVp, and 140 kVp, we have three FBP images correspondingly.

By setting $R = 3$ for Eq. (2), we have three linear equations for three basis materials with the triple energy CT FBP images μ^{E_q} (Tube voltage = E_q , $q = 1,2,3$) as follows [4],

$$\mu_j^{E_1} = \mu_1(E_1^{eff})f_{1j} + \mu_2(E_1^{eff})f_{2j} + \mu_3(E_1^{eff})f_{3j}, \quad (3a)$$

$$\mu_j^{E_2} = \mu_1(E_2^{eff})f_{1j} + \mu_2(E_2^{eff})f_{2j} + \mu_3(E_2^{eff})f_{3j}, \quad (3b)$$

$$\mu_j^{E_3} = \mu_1(E_3^{eff})f_{1j} + \mu_2(E_3^{eff})f_{2j} + \mu_3(E_3^{eff})f_{3j}, \quad (3c)$$

where E_q^{eff} denotes the effective energy of the corresponding X-ray spectrum at each selected tube voltage E_q . $\mu_1(E_q^{eff})$, $\mu_2(E_q^{eff})$, and $\mu_3(E_q^{eff})$ describes the linear attenuation coefficient for basis material soft tissue, bone, and lung tissue at each effective energy, respectively.

Hence, the fractions f of each material can be solved by minimizing the mean squared difference between the calculated attenuation coefficients with (3a)-(3c) and the reconstructed attenuation coefficients at each energy as follows,

$$\Phi(f) = \sum_{q=1}^3 \sum_{j=1}^J (\mu_j^{E_q} - \sum_{r=1}^3 \mu_r(E_q^{eff}) f_{rj})^2, \quad (4)$$

Similar to [4], a grid search method can be utilized to optimize the objective function (4) to obtain the decomposed three materials.

3.2 Virtual Monoenergetic CT images Generation

From the three basis material images obtained by the image-domain or pre-log data domain, a series of VMIs at selected n energies are generated with the corresponding tissue mass attenuation coefficients as follows. For example, we can choose $n = 10$ with the energy values of 5, 8, 10, 12, 15, 20, 25, 30, 35, 40 and 45 keV, where the HU values in this energy range of 5-45 kVp have the maximum differences among the tissues to generate the tissue contrast features for CADx. Hence, the virtual monoenergetic CT images or VMIs in the range can be expressed by,

$$\mu_j^{virtual}(\varepsilon) = \sum_r \mu_r(\varepsilon) f_{rj}, \quad (5)$$

where $\varepsilon = [5,8,10,15,20,25,30,35,40,45]$, $\mu_r(\varepsilon)$ represents the linear attenuation coefficient of r tissue type.

3.3 Machine Learning (ML)-based CADx

1) Deep learning (DL)-based CNN model:

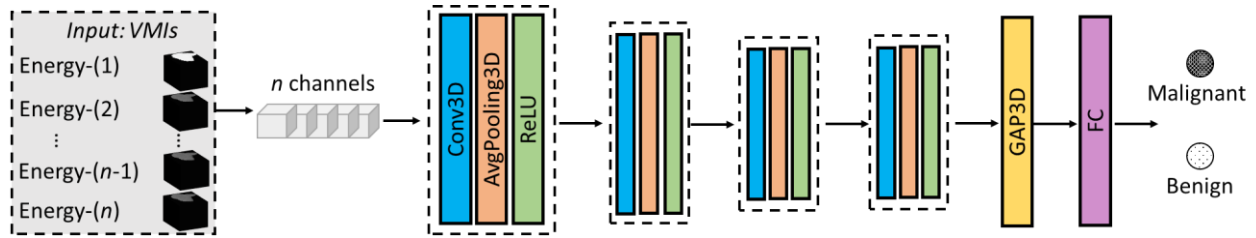


Fig. 1: The 3D CNN architecture of CADx for lung nodule diagnosis.

For the DL-based model, a 3D CNN architecture is designed, which has a multi-channel input with each energy image, as shown in Fig. 1. We first use four convolutional layers to extract the features, which are then pooled together with a global average pooling (GAP3D) layer such that the final features have a global receptive field. Then, we use a fully connected (FC) layer-based classifier to distinguish the malignant and benign lesions. Specifically, each convolutional layer consists of three operators: 3D convolution (Conv3D), 3D average pooling (Avgpooling3D), and rectified linear unit (ReLU). We adopt the binary cross-entropy loss to train the model. The details of the CNN model are listed in Table I.

TABLE I: DETAILS OF NETWORK DESIGN

Layer	Type	Channels	Kernel Size	Padding	Stride	Activation
1	Conv3D	32	(7,7,7)	(1,1,1)	(1,1,1)	ReLU
2	Avgpooling3D	-	(2,2,2)	-	(2,2,2)	-
3	Conv3D	64	(5,5,5)	(1,1,1)	(1,1,1)	ReLU
4	Avgpooling3D	-	(2,2,2)	-	(2,2,2)	-
5	Conv3D	128	(3,3,3)	(1,1,1)	(1,1,1)	ReLU
6	Avgpooling3D	-	(2,2,2)	-	(2,2,2)	-
7	Conv3D	128	(3,3,3)	(1,1,1)	(1,1,1)	ReLU
8	Avgpooling3D	-	(2,2,2)	-	(2,2,2)	-
9	GAP3D	-	-	-	-	-
10	FC	128	-	-	-	-

Based on the above model, the final classification result will show the lung nodule diagnosis performance with the explored lung tissue material spectral information in VMIs.

3. EXPERIMENTS AND RESULTS

3.1 Datasets

114 patients were scheduled for CT-guided lung nodule needle biopsy with X-ray exposure of clinical dose at 120 kVp, 100 mAs in Stony Brook University Hospital, USA. With the pathological report, a total of 114 lung nodules with 50 benign and 64 malignant were confirmed. Each CT scan covers a portion of the patient's entire chest volume, resulting in 100–200 image slices of 512×512 array size, and each image voxel is nearly cubic with an edge size of 1 mm.

3.2 Multi-energy CT Scan Simulation

In this study, we simulated the DECT and TECT scans with the above dataset. First, each slice image in the datasets was segmented as basis materials (soft tissue/bone for DECT, soft tissue/bone/lung tissue for TECT) with a simple threshold method and transferred the linear attenuation coefficient to density by dividing the corresponding material linear attenuation coefficient at 75 keV, which is the equivalent energy of 120 kVp X-ray spectrum. Hence, the material fractions images f_r were obtained. Next, a poly-energetic forward model was used to simulate the DECT scan at 80/140 kVp and TECT scan at 60/100/140 kVp by (6):

$$\tilde{N}_{wi} = \sum_{\epsilon} S_w(\epsilon) \exp\left(-\sum_j A_{ij} \sum_{r=1}^R \mu_r(\epsilon) f_{rj}\right). \quad (6)$$

An equidistant fan-beam geometry was assumed for a DECT scanner. The distance from the X-ray source to the isocenter is 570 mm and the distance from the source to the detector (SDD) is 1040 mm. 1160 projections from a full angle were acquired with 672 detector elements with a width of 1.4 mm per element. The X-ray spectrum at 60-, 80-, 100- and 140-kVp were generated by the SpekCalc software with 3mm Al filtration. Then, the multi-energy CT scan simulation was done. In this paper, all the reconstructed basis material fraction image slices have an array size of 512×512 with each pixel in the image slices covering an area of $1 \text{ mm} \times 1 \text{ mm}$. The value of β in the cost function (14) was empirically set to be 0.5 for the pre-log reconstruction.

3.3 CNN Training Implementation

For the input to the CNN-based implementation, we first converted each n -energy data with the resolution of $64 \times 64 \times 64$ voxels. And these converted energy volumetric images were fed into the multi-channel 3D CNN as shown in Fig. 1 for training. And the target is the results from the pathological reports of the malignant and benign lesions. The k -fold ($k=5$) cross-validation was implemented to test the robustness and avoid data bias. The procedure is as follows. We firstly shuffled the dataset randomly and split it into 5 folds. For each fold, we randomly divided the dataset into training and testing datasets. And then we trained a model on the training dataset and evaluated it on the testing dataset. Finally, we retained the evaluation score for each fold and the average score was calculated. In this study, the CNN model was trained for 100 epochs with a learning rate of 0.001 and batch size of 8 using Adam optimizer [5].

3.4 Lung tissue material decomposition

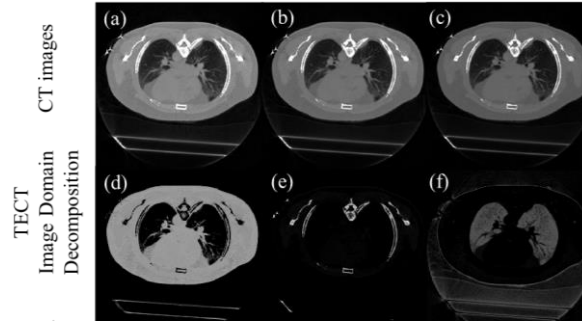


Fig. 2: Axis slice of CT images in one dataset: (a) 60 kVp, (b) 100 kVp, (c) 140kVp. Results of TECT image domain decomposition: (d) soft tissue, (e) bone, (f) lung tissue. CT images display window: $[0,0.5] \text{ cm}^{-1}$, Tissue fraction images display window: $[0,1.2]$.

Fig.2 shows the lung tissue material decomposition images from the TECT in the image domain. The result indicates that lung tissue can be reconstructed as one basis material with multi-energy CT data.

3.5 Classification Performance

With the three decomposed material fraction images from the above, the contrast-enhanced 10-energy VMIs data are generated by (18) and incorporated into the CADx part of our proposed ML-based methods. Meanwhile, to further verify the significance of lung tissue as the basis material, the traditional decomposed materials (soft tissue/bone) from DECT are also adopted to generate the VMIs for ML-based CADx. The conventional single CT data is also applied to CADx for comparison. For simplicity, we define the material decomposition methods in the image domain of DECT as **DE-FBP**, the corresponding methods of TECT as **TE-FBP**. To illustrate the effectiveness and the generality of our ML-based CADx, the AUC of each dataset was calculated.

For the DL-based CNN model, the conventional CT and the enhanced 10-energy VMI data w/ and w/o lung tissue basis material generated by different multi-energy data were incorporated into our 3D-CNN network, respectively. We calculated the mean values of AUC scores, which are shown in Table II. We have the following observations. First, the multi-energy CT data achieve higher mean AUC values than the conventional 120 kVp data, which verifies the effectiveness of the contrast enhancement brought from the VMIs. Second, by considering the lung tissue as a basis material, the results show that the mean AUC values improved 3.64% for lung nodule characterization in comparison with the image-domain method by multi-energy CT. The main reason why the VMIs with lung tissue perform well is that the lung tissue has a distinct feature from the soft tissue and brings richer information for DL-based diagnosis.

TABLE II: MEAN AUC VALUES FOR DL-BASED CNN DIAGNOSIS MODEL

Data	METHOD	Lung tissue as basis material	AUC
Conventional CT (120kVp)	FBP	-	59.54
DECT images	DE-FBP	✗	65.53
TECT images	TE-FBP	✓	69.17

4. DISCUSSION

In this study, we proposed to use lung tissue as one basis material along with soft tissue and bone with the multi-energy CT material decomposition for lung nodule characterization. The proposed CADx framework with lung tissue basis material fully utilizes the contrast enhancement at each energy bin and improves the diagnosis performance. However, there are opportunities for further refinements. First, how the decomposed image quality affects the CADx performance would be a very interesting future research. Second, for the VMIs generation, we selected 10 energies as an example. Ideally, when the basis material fraction images are well reconstructed, an arbitrary number of VMIs could be generated. Hence, it remains an interesting topic to analyze the effect of the selected energy number on the CADx performance and optimize the range and number of energies in the range. Third, the feature quality of enhanced energy images varies among each other and not all of them are guaranteed to contain meaningful features to improve the CADx performance [6]. Exploring the meaningful features from the VMIs and developing an adaptive learning model should also be further investigated as future work. Finally, clinical evaluations with more human lung data sets are needed to test the robustness of the proposed method.

5. CONCLUSIONS

In conclusion, this study proposed an end-to-end computer-aided diagnosis framework for lung nodule characterization by multi-energy CT, which fully utilizes contrast enhancement on lung tissue as a basis material in reconstruction. Experimental results demonstrated that the lung tissue is able to be decomposed by multi-energy CT data with either the image-domain. The results also indicated the advantages of the VMIs generated with lung tissue material over the VMIs without lung tissue and conventional CT images in ML-based lung nodule classification.

REFERENCES

- [1] S. Chang et al., "Spectrum estimation-guided iterative reconstruction algorithm for dual energy ct," IEEE transactions on medical imaging, vol. 39, no. 1, pp. 246-258, 2019.
- [2] W. Zhao et al., "A unified material decomposition framework for quantitative dual - and triple - energy CT imaging," Medical physics, vol. 45, no. 7, pp. 2964-2977, 2018.
- [3] M. Abella, C. Martínez, M. Desco, J. J. Vaquero, and J. A. Fessler, "Simplified Statistical Image Reconstruction for X-ray CT With Beam-Hardening Artifact Compensation," IEEE transactions on medical imaging, vol. 39, no. 1, pp. 111-118, 2019.
- [4] P. Granton, S. Pollmann, N. Ford, M. Drangova, and D. Holdsworth, "Implementation of dual - and triple - energy cone - beam micro - CT for postreconstruction material decomposition," Medical physics, vol. 35, no. 11, pp. 5030-5042, 2008.
- [5] D. P. Kingma and J. Ba, "Adam: A method for stochastic optimization," arXiv preprint arXiv:1412.6980, 2014.
- [6] S. Chang et al., "A feasibility study of computer-aided diagnosis with DECT Bayesian reconstruction for polyp classification." Medical Imaging 2022: Computer-Aided Diagnosis. Vol. 12033. SPIE, 2022.